Supplementary Material for "Rainbow Scars: From Area to Volume Law"

Christopher M. Langlett,[1] Zhi-Cheng Yang,[2,3] Julia Wildeboer,[4]
Alexey V. Gorshkov,[2,3] Thomas Iadecola,[4,*] and Shenglong Xu[1,†]

[1] *Department of Physics & Astronomy, Texas A&M University, College Station, Texas 77843, USA*
[2] *Joint Center for Quantum Information and Computer Science, NIST/University of Maryland, College Park, Maryland 20742, USA*
[3] *Joint Quantum Institute, NIST/University of Maryland, College Park, Maryland 20742, USA*
[4] *Department of Physics & Astronomy, Iowa State University, Ames, Iowa 50011, USA*

S1. RAINBOW SCAR ENTANGLEMENT ENTROPY

In this Appendix, we show that, for a random partition of the system into sub-regions A and B, the average entanglement between A and B for the rainbow state $|I\rangle$ scales extensively with the size of the smaller subregion. (Without loss of generality, we assume region A to be the smaller of the two sub-regions.) We further study the scaling of the Rényi entropy for the projected rainbow scar states of the U(1) tower in the limit of large system size N. We give results for both the standard entanglement cut and a fine-tuned cut for which the rainbow state has zero entanglement. We emphasize that the results of this Appendix also hold for the other rainbow states $|X\rangle, |Y\rangle$, and $|Z\rangle$, since these states are obtained from $|I\rangle$ by unitary operations that generate no additional entanglement.

A. Average Entanglement Entropy for a Random Bipartition

We consider the rainbow state $|I\rangle$ [see Eq. (2) in the main text] in a system of $2N$ sites. In total there are 2^{2N} possible bipartitions, since each site can be either included or excluded from region A. The size of region A for a given bipartition is $\ell = 2\,n_{\rm bp} + n_{\rm s}$ where $n_{\rm bp}$ is the number of Bell pairs enclosed in region A and $n_{\rm s}$ is the number of singleton sites (or, equivalently, the number of entanglement "bonds" cut by the bipartition). Given a bipartition, the entanglement entropy scales with the number of singletons, $S = n_{\rm s}\log(d)$ (for concreteness we set $d = 2$.). For each $\ell \in [0, 2N]$, we determine the average singleton number, $\overline{n}_{\rm s}$, as follows:

$$\overline{n}_{\rm s} = \sum_{n_{\rm s}=0}^{\ell}{}' \, n_{\rm s} P_\ell(n_{\rm s}) \tag{S1}$$

where $P_\ell(n_{\rm s})$, the probability distribution of $n_{\rm s}$ for fixed ℓ, satisfies

$$\sum_{n_{\rm s}=0}^{\ell}{}' \, P_\ell(n_{\rm s}) = 1. \tag{S2}$$

Here, the prime on the summation symbol denotes that the sum runs only over the values of $n_{\rm s}$ for which $n_{\rm bp} = (\ell - n_{\rm s})/2$ is an integer. $P_\ell(n_{\rm s})$ takes the combinatorial form

$$P_\ell(n_{\rm s}) = \frac{1}{\binom{2N}{\ell}} \binom{N}{n_{\rm bp}} \binom{N - n_{\rm bp}}{n_{\rm s}} 2^{n_{\rm s}}. \tag{S3}$$

The above expression is determined first by picking $n_{\rm bp}$ from the total number of N Bell pairs in the rainbow state. The remaining $N - n_{\rm bp}$ Bell pairs furnish the $n_{\rm s}$ singletons. The factor $2^{n_{\rm s}}$ arises from the fact that each singleton site can reside within either of subsystems 1 and 2. The remaining factor of $\binom{2N}{\ell}$ ensures normalization. Combining Eq. (S1) and Eq. (S3) results in the bipartition-averaged entanglement entropy

$$S_{\rm av} = \frac{1}{2N-1}(2N-\ell)\ell\log(2), \tag{S4}$$

which fits the numerical result in Fig. 1(a) of the main text. Note that the above expression for $S_{\rm av}$ scales extensively with system size N when $\ell \propto N$. In the large-N limit the probability distribution $P_\ell(n_{\rm s})$ approaches a Gaussian distribution of the form,

$$P_\ell(n_{\rm s}) \to \sqrt{\frac{2N}{\bar{n}_{\rm s}^2 \pi}} \exp\left(-N\frac{(n_{\rm s} - \bar{n}_{\rm s})^2}{2\bar{n}_s^2}\right), \tag{S5}$$

where the mean

$$\bar{n}_{\rm s} = \frac{1}{2N}(2N-\ell)\ell. \tag{S6}$$

The standard deviation of $n_{\rm s}/N \to 0$ as $N \to \infty$, indicates that the ratio $n_{\rm s}/N$ takes the average value for a typical bipartition. This result emphasizes that the entanglement scaling of the state $|I\rangle$ for a typical entanglement cut is extensive, in stark contrast with previous exact constructions of scar states.

* iadecola@iastate.edu
† slxu@tamu.edu

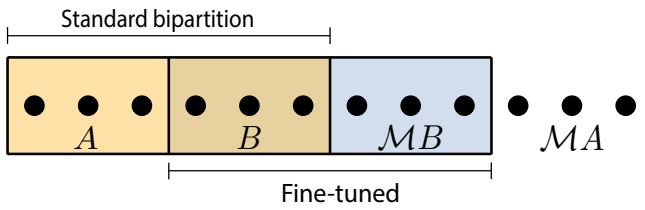

FIG. S1. *Entanglement Bipartitions.* The standard bipartition (orange) is constructed with a cut placed between sites N and $(N+1)$ and spanned by $|S^{A(B)}\rangle$ in the local S^z basis. The fine-tuned bipartition (blue) is formed by a cut between sites $(N/2, N/2+1)$, as well as, $(3N/2, 3N/2+1)$ and spanned by the basis states $|S^B\rangle$ and its mirror $|\mathcal{M}S^B\rangle$.

B. Entanglement of the U(1) Rainbow Tower

In this section we consider the rainbow scars of the XYZ model with a U(1) symmetry [Eq. (3) in the main text with $h_x = h_y = 0$ and $J_x = J_y$] and perform a large-N analysis of the Rényi entropy. When the total magnetization $S^z = \sum_{i=1}^{2N} S_i^z$ of the combined system is conserved, the Hilbert space is a direct sum of sub-sectors labelled by S^z eigenvalues $\{-N, \cdots, N\}$. We represent the rainbow scars within each magnetization sector as:

$$\begin{aligned} |\Phi_n\rangle &= \mathcal{N}(n) \left(J^+\right)^n \prod_{i=1}^{2N} |\downarrow\rangle_i \,, \\ &= \binom{N}{n}^{-1/2} \sum_S |S\rangle \otimes |\mathcal{M}S\rangle \,, \end{aligned} \tag{S7}$$

where $|S\rangle$ is in the local S^z basis for the half-chain with total magnetization $m_n = n - N/2$ with $n \in [0, \cdots, N]$. Importantly, the state $|\Phi_n\rangle$ is the sum over all permutations of n mirror excitations in a polarized background (i.e., raised spins at sites i and $\tilde{i}$). We emphasize that with each application of J^+ the number of excitations (raised spins) increases by two, resulting in the rainbow state having finite projection onto *every other* magnetization sector, leaving a tower of $(N+1)$ states. By contrast, previously studied U(1) scar towers have a non-thermal eigenstate within each magnetization sector [1, 2].

1. Standard Cut

We first consider the "standard" bipartition, where the entanglement cut is placed between sites N and $N+1$. The state (S7) is already in Schmidt-decomposed form with Schmidt coefficients

$$\lambda = \binom{N}{n}^{-1/2}, \tag{S8}$$

each with multiplicity $\binom{N}{n}$, ensuring the Schmidt coefficients are properly normalized. Therefore, the entanglement entropy takes the following form:

$$S = \log \binom{N}{n} \to -N\left((1-\gamma)\log(1-\gamma) + \gamma \log \gamma\right), \tag{S9}$$

where $\gamma = n/N$. Thus, for the standard cut the entanglement entropy scales extensively with system size, in contrast with previous examples of exact U(1) scar towers. Indeed, Eq. (S9) is the maximum possible entanglement between two quantum systems with Hilbert space dimension $\binom{N}{n}$.

2. Fine-Tuned Cut

We consider the state $|\Phi_n\rangle$ in a system of $2N$ sites, which we bipartition into regions A and B with sizes N_A and $N_B = 2N - N_A$. Here we focus on bipartitions of equal size, i.e., $N_A = N_B = N$ (we take N to be even.). Specifically, we focus on the fine-tuned bipartition where cuts are placed between sites $N/2$ and $(N/2+1)$, and between sites $3N/2$ and $(3N/2+1)$, which identifies the middle half of the system as region A. The entanglement spectrum is completely characterized by the Schmidt coefficients, which are found by first decomposing the state (S7) as

$$|\Phi_n\rangle = \sum_k \lambda_k \, |\Phi_k^A\rangle \, |\Phi_{n-k}^B\rangle \,, \tag{S10}$$

where $|\Phi_j^{A(B)}\rangle$ are a set of orthonormal states for region $A(B)$ in the local S^z basis, labelled by the number j of mirror excitations, given by

$$\begin{aligned} |\Phi_k^A\rangle &= \binom{N/2}{k}^{-1/2} \sum_{S^A} |S^A\rangle \, |\mathcal{M}S^A\rangle \\ |\Phi_{n-k}^B\rangle &= \binom{N/2}{n-k}^{-1/2} \sum_{S^B} |S^B\rangle \, |\mathcal{M}S^B\rangle \,. \end{aligned} \tag{S11}$$

The sum in $|\Phi_k^A\rangle$ is over all states $|S^A\rangle$ with magnetization $m_k = k - N/4$ in region A and the sum in $|\Phi_k^B\rangle$ is over all states $|S^B\rangle$ with magnetization $m_{n-k} = (n-k) - N/4$ in region B. The Schmidt coefficients λ_k, properly normalized, are given by

$$\lambda_k^2 = \frac{\binom{\frac{N}{2}}{k}\binom{\frac{N}{2}}{n-k}}{\binom{N}{n}}, \tag{S12}$$

and satisfy $\sum_{k=0}^{n} \lambda_k^2 = 1$. Determining the λ_k permits the construction of the Rényi entropy of order α defined as:

$$S^{(\alpha)} = \frac{1}{1-\alpha} \log \left(\sum_i \lambda_i^{2\alpha} \right), \tag{S13}$$

The Rényi entropy is then computed by taking the logarithm of the following result,

$$e^{(1-\alpha)S^{(\alpha)}} = \sum_{k=0}^{n} \frac{\binom{\frac{N}{2}}{k}^{\alpha}\binom{\frac{N}{2}}{n-k}^{\alpha}}{\binom{N}{n}^{\alpha}}. \tag{S14}$$

Using saddle point methods, the second-order ($\alpha = 2$) Rényi entropy in the large-N limit has the scaling form

$$S^{(2)} \underset{N\to\infty}{=} \frac{1}{2}\log\left(N\pi\gamma(1-\gamma)\right), \tag{S15}$$

We note that this result is different than in the case of other symmetries such as $\mathbb{Z}_2$, where the fine-tuned cut has zero entanglement; here, the scar state in each magnetization sector scales logarithmically with N provided $\gamma = n/N$ is finite.

S2. HEISENBERG PERTURBATION

We consider the consequence of perturbing the U(1)-symmetric point of two coupled Heisenberg XYZ chains composed of N spins. In the main text [see Fig. 3(d)] we demonstrated a perturbation of the form $V_{\text{pert}} = \mathcal{O}\otimes\mathbb{1} - \mathbb{1}\otimes\mathcal{O}^*$, which respects the structure of Eq. (1) but breaks the U(1) symmetry. In this instance the oscillations remain robust for perturbations strengths up to $D \sim 0.5$ before thermalization rapidly sets in. We

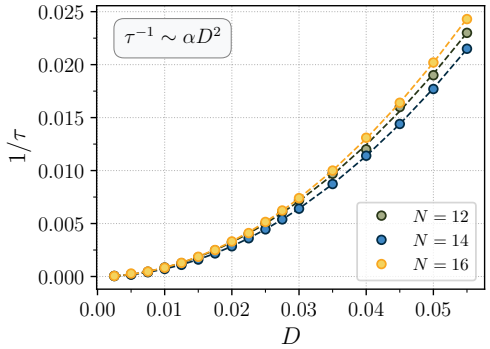

FIG. S2. (a) *Perturbation of Heisenberg XYZ model.* The inverse lifetime is extracted from fitting $\langle(S^x(t))^2\rangle/N$ with the function $f(\tau) = Ae^{-t/\tau}\cos(2\mu t) + 1/2$. The constant $\alpha \sim 6.82$ is found to be nearly twenty times larger than for the perturbation considered in the main text. The parameters used are $J_z = 2.0, J_x = J_y = 1.0, \mu = 0.5, \tilde{J} = 0.5, \lambda_c = 1.5, dt = 0.1$.

emphasize that in previous studies of perturbations of scarred models [3] the oscillations decay at much lower perturbation strengths. Therefore, the structure alone of Eq. (1) seems to act as a stabilizer of the scars' coherent dynamics without needing to add extra terms to the Hamiltonian. We confirm this suspicion by considering a perturbation which explicitly breaks the structure of Eq. (1) and the U(1) symmetry. Specifically, consider a perturbation of the form $V_{\text{pert}} = \mathcal{O}\otimes\mathbb{1} + \mathbb{1}\otimes\mathcal{O}^*$ with the operator $\mathcal{O} = \sum_i^N S_i^x S_{i+1}^x$. We extract the inverse lifetime of the oscillations' decay by fitting to a function of the form $f(\tau) = Ae^{-t/\tau}\cos(\mu t) + 1/2$ and plot it against the perturbation strength D in Fig. S2. The inverse lifetime is then fit with the function $\tau^{-1} = \alpha D^2$, which is expected from Fermi's golden rule. Surprisingly, while the perturbation considered here follows the same power law as in the main text, here the coefficient $\alpha = 6.82$ is roughly twenty times larger than the value ($\alpha = 0.4$) obtained for the perturbation considered in the main text. Due to the size of this constant, thermalization sets in at perturbation strengths ten times smaller than when the construction's structure is respected. In the future, we plan on exploring the role the structure plays in dynamics and obtain a better understanding of the constant α.

S3. RYDBERG SYSTEM

In this appendix we first study the Rydberg system from the main text in the presence of different experimental errors. For example, in order to ensure that the central sites are at the optimal detuning value, very precise laser placement is required, which generically is not perfectly accurate. As a result, some of the applied light will be imparted on the atoms directly adjacent to the two central ones, giving them a finite detuning. We study this scenario in depth and find the rainbow scar state to be robust over a wide range of parameters.

We further address the problem of state preparation by considering a the Rydberg system in the geometry of a ladder rather than a chain. Here the rainbow state is prepared on each rung of the ladder, which can be achieved with local entangling gates. Another reason why the ladder geometry is appealing is that its Hamiltonian is translation invariant.

A. Experimental Error

We now study the effects of various possible sources of error that may occur in an experimental realization of the model discussed in the main text.

As an experimental realization of rainbow scars, we studied two coupled chains of Rydberg atoms. To obtain the strongest dynamical signature of the rainbow scars, each atom should be on resonance, i.e, $\Delta_i = 0$, except for the atoms on the two central sites, where the detuning takes an optimal value Δ_{opt}. In practice, satisfying these conditions is challenging; therefore, in this appendix we study how robust the scar state is under more realistic conditions.

The first possibility we consider is to have the two central sites not set exactly at the optimal detuning; we can then define their detuning to be $\Delta = \eta\Delta_{\text{opt}}$, where $\eta \in [0, 1]$. The case $\eta = 0$ corresponds to the entire

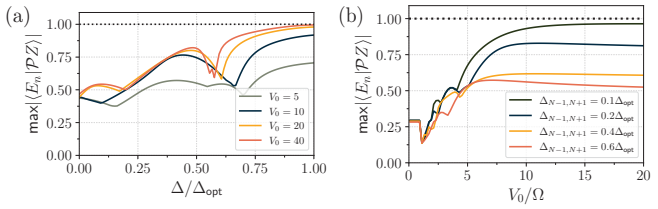

FIG. S3. *Rydberg Perturbation.* (a) Maximum overlap of $|\mathcal{P}Z\rangle$, the projection of $|Z\rangle$ into the sub-sector absent of neighboring Rydberg excitations, with all eigenstates in that sub-sector as a function of the detuning Δ on the two central sites. As Δ approaches $\Delta_{\rm opt}$ and the nearest-neighbor interaction strength V_0 is increased, the maximum overlap approaches unity. (b) Same as (a) with the detuning on the central sites fixed to $\Delta_{\rm opt}$, while the detuning on the sites directly adjacent to the central sites is fixed to different fractions of the optimal value. In this case, the maximal overlap is plotted as a function of the nearest-neighbor interaction strength V_0. Parameters used in (a), (b): $\Omega/2\pi = 2$MHz, $\Delta_{\rm opt} = V_0/2\tilde{a}^6$ with $\tilde{a} \sim 1.51$ and $2N = 12$.

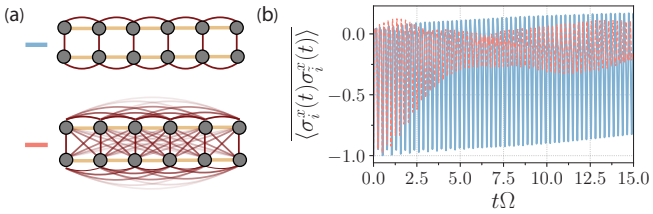

FIG. S4. *Rydberg Ladder.* (a) Cartoon depiction of the Rydberg ladder considered in Sec. S3 B for nearest-neighbor and all-to-all interactions. (b) Dynamics of the correlator $\overline{\langle\sum\sigma^x_{i,1}\sigma^x_{i,2}\rangle}$ for the initial state $|Z\rangle$, calculated using Krylov time-evolution. The parameters are: $2N = 16$, $\Omega/2\pi = 2$MHz, $V_0 = 12\Omega$, $\Delta_{\rm opt} = V_0/2\tilde{a}^6$, and $\tilde{a} \sim 1.51$.

chain being on resonance, making the chain translation-invariant except for the spacing between the two central sites. To probe the role of the detuning on the central sites, in Fig. S3(a) we plot the maximum overlap of $|\mathcal{P}Z\rangle$, the projection of the rainbow state $|Z\rangle$ into the sub-sector absent of neighboring Rydberg excitations, with all eigenstates in that sub-sector as a function of the detuning Δ on the two central sites. Surprisingly, even in the case $\eta = 0$ the maximum overlap is around fifty percent [see Fig. S3(a)], demonstrating that the signature of the scar state is *not* strictly conditioned on the detuning on the central sites being optimal. As the ratio $\Delta/\Delta_{\rm opt}$ approaches one and the interaction strength V_0 approaches infinity, the maximum overlap converges to unity in agreement with our findings in the main text.

Another possibility is error due to the coupling laser not being entirely focused on the central two sites, thereby imparting a non-zero detuning onto the sites directly adjacent to them. In Fig. S3(b) we re-calculate the maximal overlap between $|\mathcal{P}Z\rangle$ and the exact eigenstates with the detuning on sites $N-1$ and $N+2$ set to various fractions of $\Delta_{\rm opt}$. We find that, even at moderately large fractions of $\Delta_{\rm opt}$, the maximum overlap remains above fifty percent provided the nearest-neighbor interaction is sufficiently large. From an experimental perspective, these results suggest that the dynamical signature of the rainbow scars will emerge for a wide range of detunings.

B. Rydberg Ladder

In the main text we showed that, when a non-uniformly spaced Rydberg chain has its two central atoms detuned to a specific value, they become coupled by an Ising interaction, resulting in non-ergodic dynamics from a tower of rainbow scar states. While the rainbow state has a strong dynamical signature, its experimental preparation can be difficult. A possible resolution mentioned in the main text is to "fold" the chain into a ladder, which permits the use of local gates for state preparation, as well as rendering the model translation invariant. Below, we give numerical evidence that the non-ergodic signature of the rainbow scars persists in the ladder geometry under experimentally reasonable conditions. To this end, we begin with the Hamiltonian

$$H_{\parallel} = \sum_{b=1}^{2}\left(\frac{\Omega}{2}\sum_{i=1}^{N}\sigma^x_{i,b} + \sum_{i<j}V_{i,j}n_{i,b}n_{j,b}\right),$$
$$H_{\perp} = -\sum_{i=1}^{N}\sum_{b=1}^{2}\Delta_{i,b}n_{i,b} + \sum_{i,j}\tilde{V}_{i,j}n_{i,1}n_{j,2}, \tag{S16}$$

where $b = 1, 2$ labels the legs of the ladder. We set the interatomic spacing $a = 1$ between atoms on the same leg, and define $\tilde{a}$ to be the spacing between the legs. The operator σ_i^x connects the internal ground state $|g\rangle_i$ to the Rydberg state $|r\rangle_i$ of the i-th atom, with parameters Ω (Rabi frequency) and Δ_i (detuning) characterizing the drive laser. Rydberg atoms in the same leg interact through $V_{i,j} = V_0/r^6_{i,j}$, with operators $n_i = (1+\sigma_i^z)/2$. Rydberg atoms in different legs interact through $\tilde{V}_{i,j} = V_0/\tilde{r}^6_{i,j}$, where $\tilde{r}_{i,j}$ is the distance between site i in the leg $b = 1$ and site j in the leg $b = 2$. In the limit $V_{i,i+1} \gg \Omega \gg V_{i,i+2}$, we take $\tilde{V}_{i,i} = V_0/\tilde{a}^6$ to be comparable to Ω; equivalently, we take $\tilde{a} > 1.0$. By contrast to the non-uniformly spaced 1D chain, where only the middle sites are off resonance, here each rung pair is detuned to the optimal value, $\Delta_{i,1} = \Delta_{i,2} = \Delta_{\rm opt} = \tilde{V}_{i,i}/2$. With this detuning, each rung pair interacts through an Ising coupling, $V_0\sigma^z_{i,1}\sigma^z_{i,2}/4\tilde{a}^6$. In the strong-coupling limit $V_{i,i+1} \gg \Omega \gg V_{i,i+2}$, the Hilbert space splits into the sub-sectors discussed in the main text.

In this ladder geometry, the equally spaced tower of states discussed in the main text still reveals itself through the system's dynamics. We probe the presence of the tower by preparing the ladder in the $|Z\rangle$ rainbow state and, using experimentally reasonable parameters, simulate the dynamics well beyond the local relaxation

timescale, $1/\Omega$. In Fig. S4(b), we measure the expectation value $\overline{\langle \sum \sigma^x_{i,1}\sigma^x_{i,2}\rangle}$ for the case of both nearest-neighbor and all-to-all long-range interactions with parameters $V_0 = 12\Omega$ and $\tilde{a} \sim 1.51$.

In the coupled-1D-chain example discussed in the main text, the two chains interact through a single term on the center sites. Here, instead, there are N Ising couplings between the legs for nearest-neighbor interactions. Remarkably, the non-ergodic dynamics remain robust to this increase in interactions, which results from the projection of the $|Z\rangle$ rainbow state onto each sub-sector being a local eigenstate of $H_\perp$ in the strong coupling limit. Introducing long-range interactions leads to faster decay, except here the primary perturbation comes from the diagonal interaction between legs, rather than next-nearest-neighbor interactions within each leg. Despite the fact that the two sub-systems are coupled by more than a single term, the non-ergodic dynamics persists. The ladder geometry thus provides a promising alternative way to probe experimentally the dynamical signature of rainbow scars.

[1] N. O'Dea, F. Burnell, A. Chandran, and V. Khemani, From tunnels to towers: Quantum scars from lie algebras and q-deformed lie algebras, Phys. Rev. Research **2**, 043305 (2020).

[2] M. Schecter and T. Iadecola, Weak ergodicity breaking and quantum many-body scars in spin-1 xy magnets, Phys. Rev. Lett. **123**, 147201 (2019).

[3] C.-J. Lin, A. Chandran, and O. I. Motrunich, Slow thermalization of exact quantum many-body scar states under perturbations, Phys. Rev. Research **2**, 033044 (2020).